Research Article | Vol. 27, No. 5 | 4 Mar 2019 | OPTICS EXPRESS 6320
Optics EXPRESS

Ultrahigh-quality factor resonant dielectric metasurfaces based on hollow nanocuboids

J. F. Algorri,[1,*] D. C. Zografopoulos,[2] A. Ferraro,[2] B. García-Cámara,[1] R. Beccherelli,[2] and J. M. Sánchez-Pena[1]

[1]Department of Electronic Technology, Carlos III University of Madrid, Madrid 28911, Spain
[2]Consiglio Nazionale delle Ricerche, Istituto per la Microelettronica e Microsistemi (CNR-IMM), Rome 00133, Italy
[*]jalgorri@ing.uc3m.es

Abstract: In this work, a dielectric metasurface consisting of hollow dielectric nanocuboids, with ultrahigh quality factor, is theoretically proposed and demonstrated. The variation of the hole size of the cuboid allows for the tuning of the resonant anapole mode in the nanoparticles. The metasurface is designed to operate in two complementary modes, namely electromagnetically induced transparency and narrowband selective reflection. Thanks to the non-radiative nature of the anapole resonances, the minimal absorption losses of the dielectric materials, and the near-field coupling among the metasurface nanoparticles, a very high quality factor of $Q = 2.5 \times 10^6$ is achieved. The resonators are characterized by a simple bulk geometry and the subwavelength dimensions of the metasurface permit operation in the non-diffractive regime. The high quality factors and strong energy confinement of the proposed devices open new avenues of research on light-matter interactions, which may find direct applications, e.g., in non-linear devices, biological sensors, laser cavities, and optical communications.

1. Introduction

In the past decade, the study of resonant optical devices with high quality factors has attracted great attention. There are several applications for this type of devices as, for example, low-loss slow-light devices [1], the enhancement of nonlinear interactions [2], ultra-high sensitive sensing [3], narrowband filtering [4], or laser technology [5]. Devices with high quality factors are based on principles such as Fabry-Pérot resonances ($Q \sim 2 \times 10^3$) [6], photonic crystals ($Q \sim 4.5 \times 10^4$) [7], whispering gallery resonators ($Q \sim 10^9$) [8], ring resonators (for instance, $Q \sim 8 \times 10^7$ for a bend radius of $r_b = 9.65$ mm [9] and, more recently, Q $\sim 6.7 \times 10^7$ for $r_b = 369$ µm [10]), or guided-mode resonant gratings [11]. One of the main issues of the previous approaches are high volume cavities, highly delocalized optical modes and micrometric or millimeter-scale bending radii. All of these drawbacks impede the use of these devices in photonic integrated circuits (PIC) or nonlinear applications, where high confinement with low propagation losses is required. The availability of high-Q resonators (with quality factors beyond 10^7), that can be easily integrated in PIC, could create a new era in photonics technology. As commented in [9], monolithically integrated resonators and couplers allow for lithographic definition and control of the system, while further integration with other optical devices can greatly benefit from narrowband filters in the linear operation regime [12].

Several proposals have been thus far made aiming at resonant structures with small volume cavities and planar structures. Some of the most relevant are photonic crystal (PC) nanocavities and metasurfaces. In the first case, the highest experimental quality factors have been obtained in heterostructure type silicon slab nanocavities made from silicon-on-insulator (SOI) wafers [13,14]. The current record for 2D-PC nanocavities is established at $Q = 1.1 \times 10^7$ [15]. In the case of metasurfaces, a high Q-factor ($Q \sim 10^6$) has been recently demonstrated exploiting the excitation of anapole mode in arrays of metallic split ring resonators working in the gigahertz spectral

#349639 https://doi.org/10.1364/OE.27.006320
Journal © 2019 Received 31 Oct 2018; revised 19 Dec 2018; accepted 30 Dec 2018; published 20 Feb 2019

Optics EXPRESS

range [16]. The authors numerically computed $Q = 3.82 \times 10^6$, claiming this is the highest value ever achieved by theoretical metamaterials. Scaling that concept in the visible/infrared (VIS/IR) spectrum is very challenging as plasmonic metasurfaces suffer from ohmic losses inherent to metals, such that the surface resonances lead to an inevitable leak of resonant energy [17]. Similarly, the Q values of Fano resonators are often limited by ohmic damping [18].

A promising solution for high-quality factor VIS/IR resonators are all-dielectric nanostructures [19]. Their absorption losses can be minimized by properly selecting the dielectric material. For instance, the high refractive index in the most well-studied case of silicon allows for a shrinkage of the resonant volume and thus radiative decay. In parallel, the strong light confinement in high-index dielectric materials produces several multipolar resonant modes, both electric and magnetic, which span in a broad spectral range. By properly tailoring the nanoparticle shape and size, such resonators can be engineered for specific applications [20, 21]. Some interesting examples are electromagnetic-induced transparency (EIT), which relies on a Fano interference between a narrow "dark" mode resonator (low radiative loss) and a broadband "bright" mode resonator [22, 23]. When these resonances are brought close to each other in both spatial and frequency domains, their interference can result in extremely narrowband filtering in transmission [24] or reflection [35] filter.

High Q values have been demonstrated by using asymmetric configurations, such as rods ($Q \sim 10^2$) [4], ($Q \sim 6 \times 10^2$) [26], rectangular bars coupled with rings ($Q \sim 5 \times 10^2$) [27], bars ($Q \sim 2 \times 10^2$) [28], split bars ($Q \sim 10^3$) [29], and E-shaped structures with $Q \sim 10^6$ in reflective and $Q \sim 10^4$ in electrically-induced transparency (EIT) mode [30]. High-Q resonances have also been shown in symmetric configurations, for example, arrays of dielectric bars ($Q \sim 2.5 \times 10^3$) [31], or split disks on a silica glass substrate ($Q \sim 495$) [32], where it is also reported that much higher values can be achieved for nanoparticle metasurfaces embedded in a homogeneous medium ($Q \sim 10^6$). It has been recently shown that Fano resonances linked to bound states in the continuum (BIC) can yield extremely high Q-factors. For instance, cylinders [33] and meta-atoms with broken symmetry [34] have been proposed, showing $Q \sim 10^5$. In a very recent study, it was shown that by linking multipolar BIC states to the discrete states of sharp Fano resonances, ultrahigh $Q-$factors, up to 10^{10} can be obtained silicon nanodisk dimers arranged in a periodic square lattice [35].

In some of the cases illustrated, the anapole mode resonance is exploited to obtain high quality factors, which is generated due to the destructive interference of the radiation fields between electric and toroidal modes [36–40], as calculated by means of multipole decomposition in a Cartesian basis. The result of this interference is the reduction of the radiation losses, which can produce narrowband resonances analogous to EIT [41–43].

In this work, a dielectric metasurface with ultrahigh quality factor is proposed and demonstrated. The metasurface consists of hollow silicon nanoparticles in which the hole size allows to tune the anapole mode resonance. After studying several geometries, nanocuboids were observed to have the best response when they are arranged in a metasurface configuration. The metasurface resonance wavelength can be designed from EIT to a complete reflection by modifying the hole size. Thanks to the non-radiative nature of the resonances, the low absorption loss, and the near-field coupling, an ultrahigh quality factor $Q = 2.5 \times 10^6$ is demonstrated.

2. Scattering properties of hollow nanocuboids

2.1. Structural layout

The geometry of the considered nanoparticle is depicted in the inset of Fig. 1(d). It is a hollow silicon nanocuboid with square cross-section, characterized by external and internal side length equal to a and b, respectively, and thickness h. This selection was made as nanocuboids provide stronger coupling among adjacent elements in metasurface configuration with respect to the nanodisks, which are also studied as anapole-supporting nanoparticles. The central hole provides

Optics EXPRESS

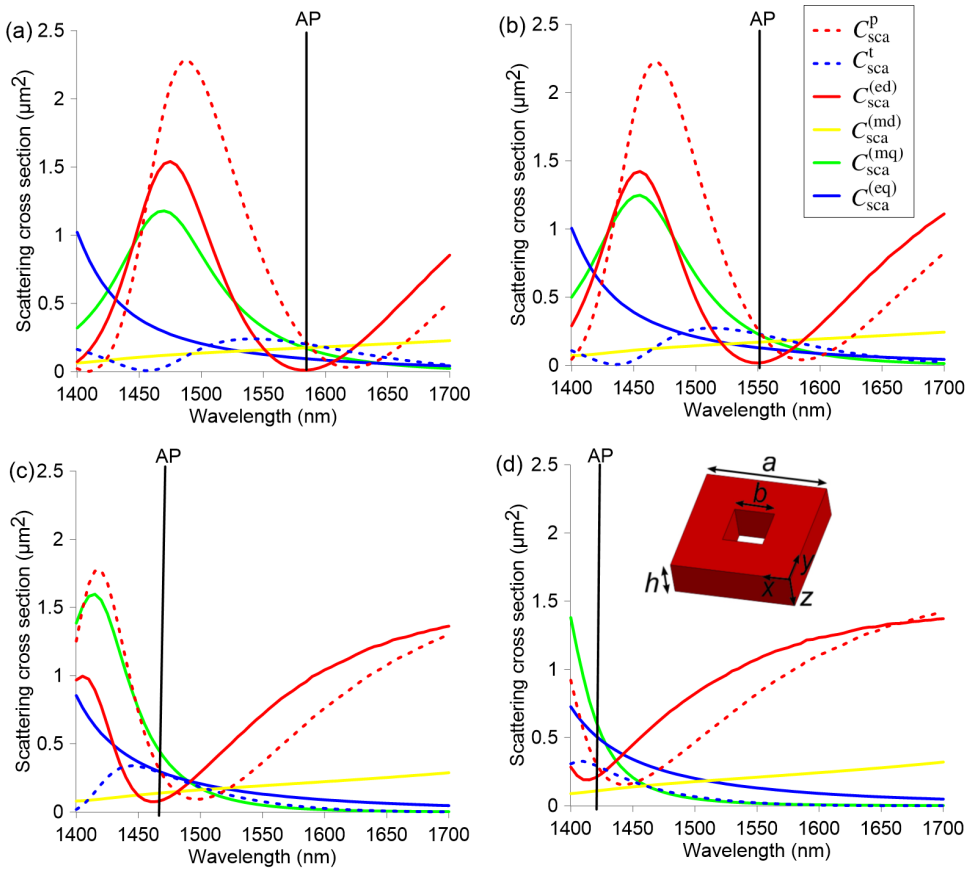

Fig. 1. Multipole decomposition and corresponding scattering cross-sections for the investigated silicon cuboid nanoparticle (a = 554 nm, h = 471 nm), for four different hole sizes (a) $b = 0$, (b) $b = 0.1a$, (c) $b = 0.2a$, (d) $b = 0.3a$.

a critical extra design parameter, which controls the field enhancement in the resonant state and its spectral position and strength, as it will be demonstrated.

As any other effect associated with the excitation of Mie resonances, the appearance of the anapole modes is directly related with the particle size and aspect ratio h/a. In this study, our design aims at maximizing the quality factor at the most widely employed wavelength in optical communication systems (λ = 1.55 μm). However, the design can be scaled in the IR spectrum, given the low material dispersion of the involved materials. It was found that only certain ranges of the aspect ratio h/a of the considered geometries may support the anapole mode, with stronger interactions for $h < a$. The dimensions of the nanocuboid were maintained subwavelength, in order to avoid diffraction of the subsequently designed metasurfaces in the target spectral window of operation. For these reasons, nanocuboids with a = 550 nm and h/a = 0.85 were selected, while the hole size was left as a free parameter to tune the resonant properties of the nanocuboids.

2.2. Multipole decomposition

The investigation of the electromagnetic and scattering properties of the nanoparticles is based on the decomposition of the fields in the dielectric nanocuboids into Cartesian multipole moments. This technique allows for the identification of the contributions stemming from toroidal moments and hence identify the conditions for anapole mode excitation [37, 44–47]. Expressed in a

Optics EXPRESS

Cartesian basis and assuming the $e^{j\omega t}$ convention for the harmonic electromagnetic fields, the induced polarization current density $\mathbf{J}(\mathbf{r})$ in the nanoparticle is given by

$$\mathbf{J}(\mathbf{r}) = j\omega\left(\varepsilon_p - \varepsilon_b\right)\mathbf{E}(\mathbf{r}), \tag{1}$$

where ω is the angular frequency, $\mathbf{E}(\mathbf{r})$ is the electric field, and $\varepsilon_p = \varepsilon_{r,p}\varepsilon_0$ and $\varepsilon_b = \varepsilon_{r,b}\varepsilon_0$ are the permittivities of the nanoparticle and the background medium, respectively, ε_0 being the vacuum permittivity. The relative permittivities $\varepsilon_{r,p}$, $\varepsilon_{r,b}$ equal the square of the corresponding refractive indices n_p, n_b of the two non-magnetic media.

The dipolar moments of the nanoparticle for the electric, magnetic, and toroidal contributions are expressed as

$$\mathbf{p} = \frac{1}{j\omega}\int_V \mathbf{J}(\mathbf{r})d\mathbf{r} \tag{2}$$

$$\mathbf{m} = \frac{1}{2\upsilon_b}\int_V \left[\mathbf{r}\times\mathbf{J}(\mathbf{r})\right]d\mathbf{r} \tag{3}$$

$$\mathbf{t} = \frac{1}{10\upsilon_b}\int_V \left[\left(\mathbf{r}\cdot\mathbf{J}(\mathbf{r})\right)\mathbf{r} - 2r^2\mathbf{J}(\mathbf{r})\right]d\mathbf{r}, \tag{4}$$

where $\upsilon_b = c/n_b$ is the speed of light in the background medium and the integral is calculated in the volume of the particle. The electric, magnetic, and toroidal quadrupole moments read as

$$Q^e_{\alpha\beta} = \frac{1}{j2\omega}\int_V \left[r_\alpha J_\beta + r_\beta J_\alpha - \frac{2}{3}\delta_{\alpha\beta}\left(\mathbf{r}\cdot\mathbf{J}(\mathbf{r})\right)\right]d\mathbf{r} \tag{5}$$

$$Q^m_{\alpha\beta} = \frac{1}{3\upsilon_b}\int_V \left\{\left[\mathbf{r}\times\mathbf{J}(\mathbf{r})\right]_\alpha r_\beta + \left[\mathbf{r}\times\mathbf{J}(\mathbf{r})\right]_\beta r_\alpha\right\}d\mathbf{r} \tag{6}$$

$$\begin{aligned} Q^T_{\alpha\beta} = \frac{1}{28\upsilon_b}\int_V \Big[&4r_\alpha r_\beta\left(\mathbf{r}\cdot\mathbf{J}(\mathbf{r})\right) - 5r^2\left(r_\alpha J_\beta + r_\beta J_\alpha\right) \\ &+ 2r^2\delta_{\alpha\beta}\left(\mathbf{r}\cdot\mathbf{J}(\mathbf{r})\right)\Big]d\mathbf{r}, \end{aligned} \tag{7}$$

where δ is the Dirac delta function and the subscripts $\alpha, \beta = x, y, z$. The mean-square radii corrections for the magnetic and toroidal dipole distributions are given by

$$\overline{\mathbf{R}}^2_m = \frac{1}{2\upsilon_b}\int_V \left[\mathbf{r}\times\mathbf{J}(\mathbf{r})\right]r^2 d\mathbf{r}, \tag{8}$$

$$\overline{\mathbf{R}}^2_t = \frac{1}{28\upsilon_b}\int_V \left[3r^2\mathbf{J}(\mathbf{r}) - 2r\left(\mathbf{r}\cdot\mathbf{J}(\mathbf{r})\right)\right]r^2 d\mathbf{r}. \tag{9}$$

The mean-square radius correction for the electric dipole component has been omitted, as it does not contribute to the far-field radiation [44].

The partial scattering cross-sections associated with each multipole moment are given by

$$C^{(\mathrm{ed})}_{\mathrm{sca}} = \frac{k_b^4}{6\pi\varepsilon_b^2}\left|\mathbf{p} - jk_b\left(\mathbf{t} + \frac{k_b^2}{10}\overline{\mathbf{R}}^2_t\right)\right|^2, \tag{10}$$

$$C^{(\mathrm{md})}_{\mathrm{sca}} = \frac{k_b^4}{6\pi\varepsilon_b^2}\left|\mathbf{m} - \frac{k_b^2}{10}\overline{\mathbf{R}}^2_m\right|^2 \tag{11}$$

$$C^{(\mathrm{eq})}_{\mathrm{sca}} = \frac{k_b^6}{20\pi\varepsilon_b^2}\sum_{\alpha\beta}\left|Q^e_{\alpha\beta} - j\frac{k_b}{3}Q^T_{\alpha\beta}\right|^2 \tag{12}$$

Optics EXPRESS

$$C_{\mathrm{sca}}^{(\mathrm{mq})} = \frac{k_b^6}{80\pi\varepsilon_b^2}\sum_{\alpha\beta}\left|Q_{\alpha\beta}^m\right|^2, \tag{13}$$

assuming $|\mathbf{E}_0| = 1$ V/m for the electric field amplitude of the incident plane wave.

It is convenient to define also the magnitudes $C_{\mathrm{sca}}^{\mathrm{p}}$ and $C_{\mathrm{sca}}^{\mathrm{t}}$

$$C_{\mathrm{sca}}^{\mathrm{p}} = \frac{k_b^4}{6\pi\varepsilon_b^2}|\mathbf{p}|^2 \tag{14}$$

$$C_{\mathrm{sca}}^{\mathrm{t}} = \frac{k_b^6}{6\pi\varepsilon_b^2}\left|\mathbf{t} + \frac{k_b^2}{10}\overline{\overline{\mathbf{R}}}_t^2\right|^2, \tag{15}$$

which correspond to effective cross-sections of the Cartesian electric and toroidal dipoles, respectively. These two dipoles may interfere constructively or destructively, depending on their relative phase difference, and their combined contribution to the electric dipole scattering cross-section is described in Eq. (10). Nevertheless, the separate calculation of Eqs. (14)-(15) facilitates the design of the proposed structures and provides further insight on the excitation of the anapole modes, which occurs at a crossover of $C_{\mathrm{sca}}^{\mathrm{p}}$ and $C_{\mathrm{sca}}^{\mathrm{t}}$.

2.3. Results

The results of the multipole decomposition for the investigated nanocuboids for four cases with respect to the hole size are shown in Fig. 1. The surrounding medium is air and the excitation field is a y-polarized plane wave propagating along the z-axis. The material dispersion of silicon was taken into account [48]. All simulations were carried out by means of the finite-element method (FEM), implemented in the commercial software Comsol Multiphysics$^{\mathrm{TM}}$. The anapole mode stems from the destructive interference between Cartesian electric and the toroidal dipoles, as discussed in Subsection 2.2, and the corresponding wavelengths are marked in the graphs with the annotation "AP", which also coincides with the minimum of the total electric dipole cross-section, given by Eq. (10). The inclusion of the hole in the nanocuboid produces a significant shift to shorter wavelengths for the anapole, indicating that it is an efficient means of controlling its spectral position. The magnetic dipole is weak and stays almost constant in the considered spectrum range.

Figure 2 shows the profiles of the relative enhancement of the electric and magnetic near-fields calculated at the x-y and x-z mid-planes of the nanocuboid, respectively. The profiles are calculated at the wavelengths corresponding to the anapole modes for the $b = 0$ (solid nanocuboid) and $b = 0.2a$ cases, as investigated in Figs. 1(a) and 1(c). The characteristic electric and magnetic line profiles, namely opposite circular displacement currents at the nanocuboid sides and a perpendicular circular magnetic moment distribution, stem from the interfering electric and toroidal dipoles that generate the anapole mode, as further corroborated by the observed field enhancement [42, 49].

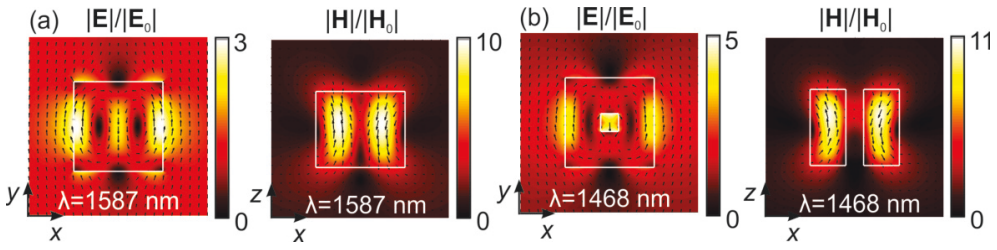

Fig. 2. Electric and magnetic field enhancement profiles at the anapole resonant wavelengths for (a) $b = 0$ and (b) $b = 0.2a$.

Optics EXPRESS

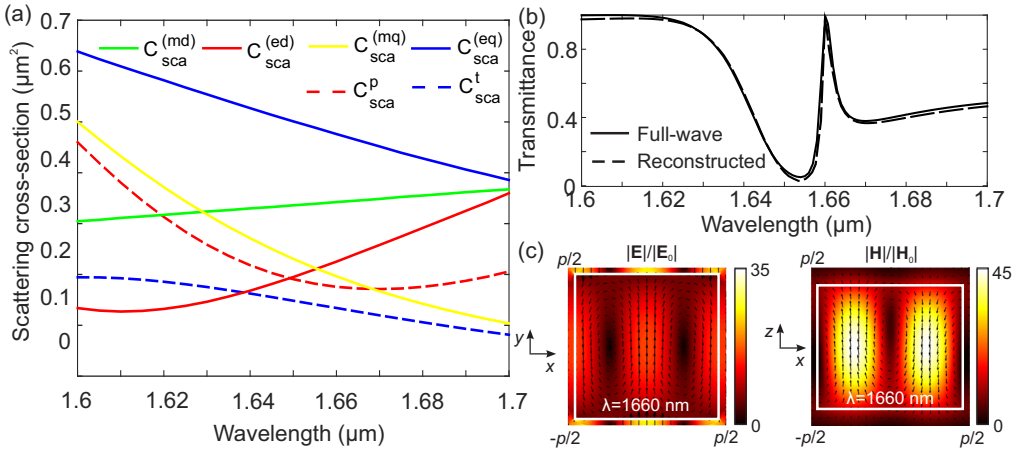

Fig. 3. (a) Scattering cross-section of the multipole modes for a solid silicon nanocuboid (a = 554 nm, h = 471 nm), embedded in a dielectric medium with n_b = 1.4. (b) Transmittance of a square periodic metasurface array with pitch p = 604 nm composed of the nanocuboids studied in (a), calculated via full-wave simulations and by reconstructing the electric field from the multipole contributions. (c) Electric and magnetic field enhancement profiles at the metasurface resonant wavelength of 1660 nm.

3. Resonant dielectric metasurfaces of hollow nanocuboids

The investigated metasurfaces are composed of silicon hollow nanocuboids arranged in a periodic array with pitch p. The metasurface is patterned on a glass substrate, the commercial optical glass Borofloat 33, characterized by an index of n = 1.456 at 1.55 μm. The metasurface is then covered by a thick layer of polydimethylsiloxane (PDMS) with n = 1.396 at 1.55 μm, as shown in the inset of Fig. 4, to protect the structure and ensure quasi-matching of the refractive index between substrate and superstratum, which enables more efficient amplitude matching among resonant modes [46]. Both materials show negligible material dispersion in the considered IR spectral window.

As a first remark, it was verified that the presence of a surrounding medium shifted the anapole modes towards higher wavelengths, which was an expected behaviour. Figure 3(a) investigates the scattering cross-sections of the multipole modes for a solid nanocuboid with dimensions as in Fig. 1(a), but embedded in a homogeneous medium with n_b = 1.4. The appearance of strong resonances is in this case hindered due to the lower dielectric permittivity contrast $\varepsilon_p/\varepsilon_b$, which leads to broader, overlapping spectra. The Cartesian toroidal and electric dipole spectra do not cross, but the difference of their cross-sections reaches a minimum at 1660 nm. However, in a metasurface configuration the radiative damping can be minimized thanks to collective oscillations mediated by near-field coupling between the nanoparticles [27, 50, 51], the key parameter of the design being the value of the metasurface pitch. In this respect, the rectangular shape of the nanocuboids makes this coupling higher than in the case of nanodisks. Since large separation values $s = p - a$ lead to weaker resonances, here a value of s = 50 nm is considered, which was shown to provide sharp resonances in a broad background spectrum.

Figure 3(b) investigates the reference case of a metasurface composed of the solid nanocuboids of Fig. 3(a) arranged in a square lattice of pitch p = 604 nm. The transmittance spectrum was calculated via i) full-wave FEM simulation and ii) by reconstructing the field from the multipole contributions as defined in Section 2, but calculated at the metasurface unit cell, following the procedure described in [37]. Very good agreement is observed; the minor difference is attributed to the omission of square-mean radii corrections for the quadrupole modes and the truncation of

Optics EXPRESS

the multipole series. The presence of the strong resonance at 1660 nm stems from the excitation of the toroidal mode, as evidenced by the electric and magnetic field enhancement profiles shown in Fig. 3(c) [32].

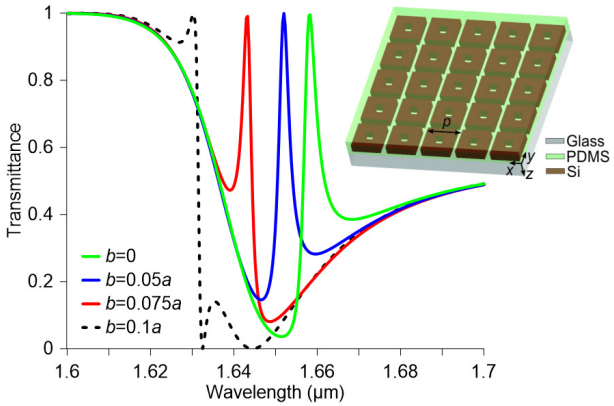

Fig. 4. Transmittance of the metasurface for several hole sizes (b ranging from 0 to $0.1a$). The dimensions of the silicon nanocuboids are $a = 554$ nm and $h = 471$ nm and the pitch of the metasurface is $p = 604$ nm.

The transmittance T of a metasurface with the same dimensions as in the case of Fig. 3(b), but considering the realistic glass/PDMS substrate/superstratum is investigated in Fig. 4 for hole size varying from $b = 0$ to $b = 0.1a$. Although not shown, the reflectance can be directly calculated as $R = 1 - T$ since the absorption loss in the materials is negligible and no propagating diffraction orders exist in the spectral window under study. In all four examined cases two resonant modes can be detected, whose interference leads to an asymmetric Fano profile. Such profile results from the coupling between the broader, less sensitive to the hole size variation, "bright" electric dipole, and the subradiant "dark" toroidal dipole mode [27,32]. For the case of of $b = 0.05a$, the two interfering modes become almost degenerate leading to an EIT response [24].

In previous works, it has been shown that, apart from the radiative damping of the subradiant mode, the quality factor is determined by the coupling coefficient of two interfering modes and it increases with the reduction of the coupling [27]. An improved quality factor and strong near-field enhancements was recently achieved by adjusting the gap width for the split disk arrays [32]. A similar effect is here observed due to the hollow shape of the nanocuboids. By increasing the hole size, the resonance wavelengths of both interfering modes shift to shorter wavelengths towards the target telecom range, but the subradiant mode shifts much more rapidly compared with that of the electric dipole mode.

This is observed in Fig. 5, which investigates the metasurface response for larger hole sizes. The anapole subradiant mode shifts to a spectral window of increased background transmittance, stemming from the weak excitation of other modes. The resulting Fano interference results in narrowband reflection at the resonant wavelength [25], contrary to the EIT-like transmittance evidenced in Fig. 4. More importantly, the quality factor is dramatically increased due to the weak coupling of the interfering modes, which leads to very high confinement of the electromagnetic field in the near-field zone. For the designed metasurface parameters and by properly selecting the hole size ($b = 0.21a$) the maximum quality factor is reached in the vicinity of the target wavelength $\lambda = 1.55$ μm. Simulations showed that the quality factor is maximized for the considered value of separation $s = 50$ nm, while the values start to drop significantly for $s > 100$ nm.

The quality factor was calculated as the ratio between the central resonant frequency and the bandwidth, namely the range of frequencies for which the transmittance is at least half its

Optics EXPRESS

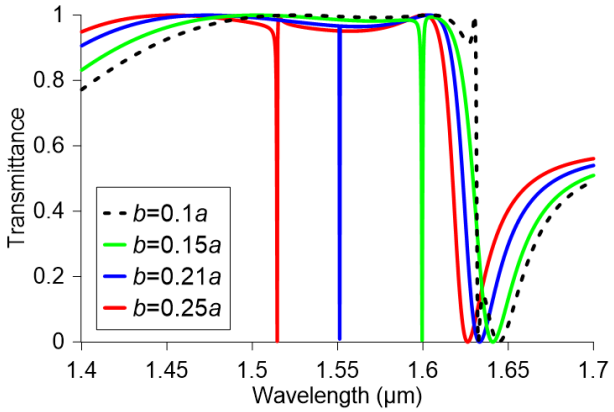

Fig. 5. Transmittance of the metasurface for several hole sizes (from $b = 0.1a$ to $b = 0.3a$). The rest of the parameters are as in Fig. 4.

maximum value. Figure 6 provides insight in this respect, providing the zoomed transmittance spectra for the critical value $b = 0.21a$ and slight deviations around it. The calculated quality factors are equal to 10^5, 2.5×10^6, and 0.5×10^5 for a hole side of $0.2a$, $0.21a$, and $0.22a$, respectively. Figure 6(a) shows the electric field enhancement on- and off-resonance. At resonance, the enhancement factor reaches values above 2000 at the internal walls of the hollow nanocuboids and in the gaps separating adjacent nanoparticles. This is three orders of magnitude higher than the values calculated off-resonance, which demonstrates the strongly confined nature of the resonance with associated very low radiative decay rates and hence the observed high quality factors.

As observed in Fig. 6, the $Q-$factor is maximized at $b = 0.21a$, which corresponds to a resonance with the most symmetric lineshape among the cases examined. In order to verify this, we have fitted the transmittance spectra of Fig. 6 with the Fano formula [52]

$$T(\omega_n) = C\frac{(F\gamma_n + \omega_n - 1)^2}{(\omega_n - 1)^2 + \gamma_n^2}, \tag{16}$$

where $\omega_n = \omega/\omega_0$ is the normalized angular frequency, $\omega_0 = 2\pi f/\lambda_{\text{res}}$, λ_{res} is the resonant wavelength, γ_n describes the normalized linewidth of the resonance, F is the Fano parameter, expressing the degree of asymmetry, and C a normalization constant. The fitted spectra, denoted with dashed lines in Fig. 6, excellently reproduce the transmittance spectra calculated via full-wave simulations, for the following set of parameters, corresponding to $b_1 = 0.2a$, $b_2 = 0.21a$, and $b_3 = 0.22a$, respectively: $C_1 = 0.965$, $C_2 = 0.963$, $C_3 = 0.965$, $\gamma_{n1} = 4.32 \times 10^{-6}$, $\gamma_{n2} = 1.656 \times 10^{-7}$, $\gamma_{n3} = 1.026 \times 10^{-5}$, and $F_1 = -0.184$, $F_2 = -0.043$, $F_3 = -0.176$.

The excellent fitting results confirm the Fano nature of the observed resonance, which stems from the interference of the sharp resonance of toroidal nature at λ_{res} with the broad sub-radiant, high-transmittance background, as evidenced in Fig. 5 from 1.4 μm to 1.6 μm. Moreover, it is verified that the value $b_2 = 0.21a$ leads to quasi-symmetric profile ($F = 0$ corresponds to perfectly symmetric Fano lineshape). Moreover, it implies that by further fine-tuning of the geometrical parameters of the structure, more symmetric profiles and hence even higher $Q-$factors might be available. Nevertheless, this analysis has been omitted, as the considered step of $0.01a$, i.e. approximately 5 nm, is already very challenging from the fabrication point of view and poses a realistic limit. Indeed, in a recent work, a silicon dimer metasurface was optimized to yield an extremely high $Q-$factor in the order of 10^{10}, which however drops by orders of magnitude for deviations of a couple of nanometers from the optimized dimensions [35].

Optics EXPRESS

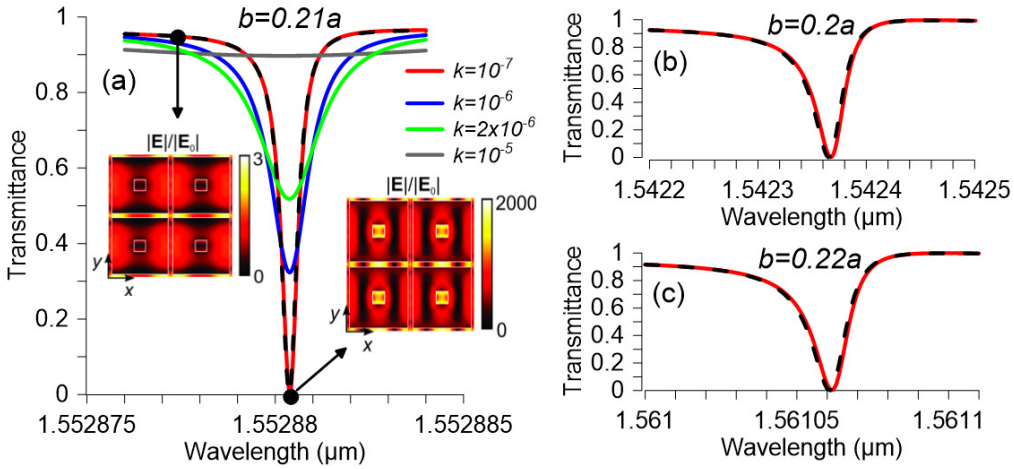

Fig. 6. Transmittance of the metasurface for three hole sizes (a) $b = 0.2a$, (b) $0.21a$, and (c) $0.22a$. For $b = 0.21a$ a maximum quality factor of $Q = 2.5 \times 10^6$ is achieved close to the target wavelength of 1.55 μm. The dashed lines are the fit to the Fano formula of Eq. 16. The effect of the losses of the dielectric nanoparticles is investigated in (a).

Finally, it is to be expected that in such strongly resonant structures the effect of material losses plays a critical role. Although polycrystalline silicon presents negligible losses in the investigated wavelength spectrum, in practice absorption and/or scattering losses can be introduced by defects or due to surface roughness during fabrication. The effect of losses is quantified by adding an imaginary part k to the Si refractive index and investigated in Fig. 6(a). In the range $0 < k < 10^{-7}$, which is well within the results of experimental characterization of silicon [53], the metasurface response is not affected. Larger values progressively deteriorate the Q-factor and also reduce the reflectance on resonance, which ceases to manifest for $k > 10^{-5}$.

4. Conclusions

In summary, a dielectric metasurface based on silicon hollow nanocuboids exhibiting very high-quality factor resonances was designed and demonstrated. The resonances arise due to the interference between toroidal anapole modes in the individual nanocuboids and the metasurface collective modes. The spectral position of the anapoles is controlled by adjusting the hole size of the nanocuboids. Through proper design, the metasurface can operate in an EIT-like regime or as a very narrowband notch filter in reflection. Thanks to the non-radiative nature of the resonance, the negligible absorption loss and the near field coupling on the metasurface, a very high quality factor of $Q = 2.5 \times 10^6$ is demonstrated at the telecom relevant wavelength of 1.55 μm. The proposed structure can find direct application in systems relying on strong light-matter interactions, such as non-linear devices, biological sensors, or on narrowband filtering, e.g., in laser cavities or optical communications.

Funding

Research and Development Program through the Comunidad de Madrid (SINFOTON S2013/MIT-2790); Ministerio de Economía y Competitividad of Spain (TEC2013-47342-C2-2-R); mobility programs of Carlos III University and "José Castillejo" of the Ministerio de Educación, Cultura y Deporte of Spain.

Optics EXPRESS

References

1. J. Gu, R. Singh, X. Liu, X. Zhang, Y. Ma, S. Zhang, S. A. Maier, Z. Tian, A. K. Azad, H.-T. Chen, A. J. Taylor, J. Han, and W. Zhang, "Active control of electromagnetically induced transparency analogue in terahertz metamaterials," Nat. Commun. **3**, 1151 (2012).
2. Y. Sun, Y.-W. Tong, C.-H. Xue, Y.-Q. Ding, Y.-H. Li, H. Jiang, and H. Chen, "Electromagnetic diode based on nonlinear electromagnetically induced transparency in metamaterials," Appl. Phys. Lett. **103**, 091904 (2013).
3. R. Singh, W. Cao, I. Al-Naib, L. Cong, W. Withayachumnankul, and W. Zhang, "Ultrasensitive terahertz sensing with high-Q Fano resonances in metasurfaces," Appl. Phys. Lett. **105**, 171101 (2014).
4. C. Wu, N. Arju, G. Kelp, J. A. Fan, J. Dominguez, E. Gonzales, E. Tutuc, I. Brener, and G. Shvets, "Spectrally selective chiral silicon metasurfaces based on infrared Fano resonances," Nat. Commun. **5**, 3892 (2014).
5. Q. Zhang, S. T. Ha, X. Liu, T. C. Sum, and Q. Xiong, "Room-temperature near-infrared high-Q perovskite whispering-gallery planar nanolasers," Nano Lett. **14**, 5995–6001 (2014).
6. X. Chen, C. Chardin, K. Makles, C. Caër, S. Chua, R. Braive, I. Robert-Philip, T. Briant, P.-F. Cohadon, A. Heidmann, T. Jacqmin, and S. Deléglise, "High-finesse Fabry-Perot cavities with bidimensional Si_3N_4 photonic-crystal slabs," Light. Sci. Appl. **6**, e16190 (2016).
7. M. S. Mohamed, A. Simbula, J.-F. Carlin, M. Minkov, D. Gerace, V. Savona, N. Grandjean, M. Galli, and R. Houdré, "Efficient continuous-wave nonlinear frequency conversion in high-Q gallium nitride photonic crystal cavities on silicon," APL Photonics **2**, 031301 (2017).
8. M. R. Foreman, J. D. Swaim, and F. Vollmer, "Whispering gallery mode sensors," Adv. Opt. Photonics **7**, 168–240 (2015).
9. D. T. Spencer, J. F. Bauters, M. J. R. Heck, and J. E. Bowers, "Integrated waveguide coupled Si_3N_4 resonators in the ultrahigh-Q regime," Optica **1**, 153–157 (2014).
10. X. Ji, F. A. S. Barbosa, S. P. Roberts, A. Dutt, J. Cardenas, Y. Okawachi, A. Bryant, A. L. Gaeta, and M. Lipson, "Ultra-low-loss on-chip resonators with sub-milliwatt parametric oscillation threshold," Optica **4**, 619–624 (2017).
11. G. Quaranta, G. Basset, O. J. F. Martin, and B. Gallinet, "Recent advances in resonant waveguide gratings," Laser Photonics Rev. **12**, 1800017 (2018).
12. P. Del'Haye, A. Schliesser, O. Arcizet, T. Wilken, R. Holzwarth, and T. J. Kippenberg, "Optical frequency comb generation from a monolithic microresonator," Nature **450**, 1214–1217 (2007).
13. Y. Taguchi, Y. Takahashi, Y. Sato, T. Asano, and S. Noda, "Statistical studies of photonic heterostructure nanocavities with an average Q factor of three million," Opt. Express **19**, 11916–11921 (2011).
14. H. Sekoguchi, Y. Takahashi, T. Asano, and S. Noda, "Photonic crystal nanocavity with a Q-factor of ~9 million," Opt. Express **22**, 916–924 (2014).
15. T. Asano, Y. Ochi, Y. Takahashi, K. Kishimoto, and S. Noda, "Photonic crystal nanocavity with a Q factor exceeding eleven million," Opt. Express **25**, 1769–1777 (2017).
16. A. A. Basharin, V. Chuguevsky, N. Volsky, M. Kafesaki, and E. N. Economou, "Extremely high Q-factor metamaterials due to anapole excitation," Phys. Rev. B **95**, 035104 (2017).
17. I. Staude and J. Schilling, "Metamaterial-inspired silicon nanophotonics," Nat. Photonics **11**, 274–284 (2017).
18. G. Dayal, X. Y. Chin, C. Soci, and R. Singh, "High-Q whispering-gallery-mode-based plasmonic Fano resonances in coupled metallic metasurfaces at near infrared frequencies," Adv. Opt. Mater. **4**, 1295–1301 (2016).
19. A. I. Kuznetsov, A. E. Miroshnichenko, M. L. Brongersma, Y. S. Kivshar, and B. Luk'yanchuk, "Optically resonant dielectric nanostructures," Science **354**, aag2472 (2016).
20. B. García-Cámara, J. F. Algorri, A. Cuadrado, V. Urruchi, J. M. Sánchez-Pena, R. Serna, and R. Vergaz, "All-optical nanometric switch based on the directional scattering of semiconductor nanoparticles," J. Phys. Chem. C **119**, 19558–19564 (2015).
21. J. Algorri, B. García-Cámara, A. Cuadrado, J. Sánchez-Pena, and R. Vergaz, "Selective dielectric metasurfaces based on directional conditions of silicon nanopillars," Nanomater. **7**, 177 (2017).
22. U. Fano, "Effects of configuration interaction on intensities and phase shifts," Phys. Rev. **124**, 1866–1878 (1961).
23. B. Luk'yanchuk, N. I. Zheludev, S. A. Maier, N. J. Halas, P. Nordlander, H. Giessen, and C. T. Chong, "The Fano resonance in plasmonic nanostructures and metamaterials," Nat. Mater. **9**, 707–715 (2010).
24. N. Papasimakis, V. A. Fedotov, N. I. Zheludev, and S. L. Prosvirnin, "Metamaterial analog of electromagnetically induced transparency," Phys. Rev. Lett. **101**, 253903 (2008).
25. N. Liu, T. Weiss, M. Mesch, L. Langguth, U. Eigenthaler, M. Hirscher, C. Sönnichsen, and H. Giessen, "Planar metamaterial analogue of electromagnetically induced transparency for plasmonic sensing," Nano Lett. **10**, 1103–1107 (2010).
26. S. Campione, S. Liu, L. I. Basilio, L. K. Warne, W. L. Langston, T. S. Luk, J. R. Wendt, J. L. Reno, G. A. Keeler, I. Brener, and M. B. Sinclair, "Broken symmetry dielectric resonators for high quality factor Fano metasurfaces," ACS Photon. **3**, 2362–2367 (2016).
27. Y. Yang, I. I. Kravchenko, D. P. Briggs, and J. Valentine, "All-dielectric metasurface analogue of electromagnetically induced transparency," Nat. Commun. **5**, 5753 (2014).
28. J. Zhang, K. F. MacDonald, and N. I. Zheludev, "Near-infrared trapped mode magnetic resonance in an all-dielectric metamaterial," Opt. Express **21**, 26721–26728 (2013).
29. J. Zhang, W. Liu, Z. Zhu, X. Yuan, and S. Qin, "Strong field enhancement and light-matter interactions with all-dielectric metamaterials based on split bar resonators," Opt. Express **22**, 30889–30898 (2014).

Optics EXPRESS

30. B. Han, X. Li, C. Sui, J. Diao, X. Jing, and Z. Hong, "Analog of electromagnetically induced transparency in an E-shaped all-dielectric metasurface based on toroidal dipolar response," Opt. Mater. Express **8**, 2197–2207 (2018).
31. C. Sui, X. Li, T. Lang, X. Jing, J. Liu, and Z. Hong, "High Q-factor resonance in a symmetric array of all-dielectric bars," Appl. Sci. **8**, 161 (2018).
32. S.-D. Liu, Z.-X. Wang, W.-J. Wang, J.-D. Chen, and Z.-H. Chen, "High Q-factor with the excitation of anapole modes in dielectric split nanodisk arrays," Opt. Express **25**, 22375–22387 (2017).
33. A. A. Bogdanov, K. L. Koshelev, P. V. Kapitanova, M. V. Rybin, S. A. Gladyshev, Z. F. Sadrieva, K. B. Samusev, Y. S. Kivshar, and M. F. Limonov, "Bound states in the continuum and Fano resonances in the strong mode coupling regime," arXiv:1805.09265 (2018).
34. K. Koshelev, S. Lepeshov, M. Liu, A. Bogdanov, and Y. Kivshar, "Asymmetric metasurfaces with high-Q resonances governed by bound states in the continuum," Phys. Rev. Lett. **121**, 193903 (2018).
35. Y. He, G. Guo, T. Feng, Y. Xu, and A. E. Miroshnichenko, "Toroidal dipole bound states in the continuum," Phys. Rev. B **98**, 161112(R) (2018).
36. T. Kaelberer, V. A. Fedotov, N. Papasimakis, D. P. Tsai, and N. I. Zheludev, "Toroidal dipolar response in a metamaterial," Science **330**, 1510–1512 (2010).
37. V. Savinov, V. A. Fedotov, and N. I. Zheludev, "Toroidal dipolar excitation and macroscopic electromagnetic properties of metamaterials," Phys. Rev. B **89**, 205112 (2014).
38. N. Papasimakis, V. A. Fedotov, V. Savinov, T. A. Raybould, and N. I. Zheludev, "Electromagnetic toroidal excitations in matter and free space," Nat. Mater. **15**, 263–271 (2016).
39. A. C. Tasolamprou, O. Tsilipakos, M. Kafesaki, C. M. Soukoulis, and E. N. Economou, "Toroidal eigenmodes in all-dielectric metamolecules," Phys. Rev. B **94**, 205433 (2016).
40. O. Tsilipakos, A. C. Tasolamprou, T. Koschny, M. Kafesaki, E. N. Economou, and C. M. Soukoulis, "Pairing toroidal and magnetic dipole resonances in elliptic dielectric rod metasurfaces for reconfigurable wavefront manipulation in reflection," Adv. Opt. Mater. **6**, 1800633 (2018).
41. V. A. Fedotov, A. V. Rogacheva, V. Savinov, D. P. Tsai, and N. I. Zheludev, "Resonant transparency and non-trivial non-radiating excitations in toroidal metamaterials," Sci. Rep. **3**, 2967 (2013).
42. A. E. Miroshnichenko, A. B. Evlyukhin, Y. F. Yu, R. M. Bakker, A. Chipouline, A. I. Kuznetsov, B. Luk'yanchuk, B. N. Chichkov, and Y. S. Kivshar, "Nonradiating anapole modes in dielectric nanoparticles," Nat. Commun. **6**, 8069 (2015).
43. W. Liu, J. Zhang, B. Lei, H. Hu, and A. E. Miroshnichenko, "Invisible nanowires with interfering electric and toroidal dipoles," Opt. Lett. **40**, 2293–2296 (2015).
44. E. E. Radescu and G. Vaman, "Exact calculation of the angular momentum loss, recoil force, and radiation intensity for an arbitrary source in terms of electric, magnetic, and toroid multipoles," Phys. Rev. E **65**, 046609 (2002).
45. E. Radescu Jr. and G. Vaman, "Cartesian multipole expansions and tensorial identities," Prog. Electromagn. Res. B **36**, 89–111 (2012).
46. Y. F. Yu, A. Y. Zhu, R. Paniagua-Domínguez, Y. H. Fu, B. Luk'yanchuk, and A. I. Kuznetsov, "High-transmission dielectric metasurface with 2π phase control at visible wavelengths," Laser Photon. Rev. **9**, 412–418 (2015).
47. A. B. Evlyukhin, T. Fischer, C. Reinhardt, and B. N. Chichkov, "Optical theorem and multipole scattering of light by arbitrarily shaped nanoparticles," Phys. Rev. B **94**, 205434 (2016).
48. E. D. Palik, ed., *Handbook of optical constants of solids* (Academic Press, 1997).
49. R. Wang and L. D. Negro, "Engineering non-radiative anapole modes for broadband absorption enhancement of light," Opt. Express **24**, 19048–19062 (2016).
50. V. A. Fedotov, N. Papasimakis, E. Plum, A. Bitzer, M. Walther, P. Kuo, D. P. Tsai, and N. I. Zheludev, "Spectral collapse in ensembles of metamolecules," Phys. Rev. Lett. **104**, 223901 (2010).
51. Y. Yang, W. Wang, A. Boulesbaa, I. I. Kravchenko, D. P. Briggs, A. Puretzky, D. Geohegan, and J. Valentine, "Nonlinear Fano-resonant dielectric metasurfaces," Nano Lett. **15**, 7388–7393 (2015).
52. G. Dayal, X. Y. Chin, C. Soci, and R. Singh, "Independent tailoring of super-radiant and sub-radiant modes in high-Q plasmonic Fano resonant metasurfaces," Adv.Opt. Mater. **4**, 1860–1866 (2016).
53. C. Schinke, P. C. Peest, J. Schmidt, R. Brendel, K. Bothe, M. R. Vogt, I. Kröger, S. Winter, A. Schirmacher, S. Lim, H. T. Nguyen, and D. MacDonald, "Uncertainty analysis for the coefficient of band-to-band absorption of crystalline silicon," AIP Adv. **5**, 067168 (2015).